Calhoun: The NPS Institutional Archive

DSpace Repository

Faculty and Researchers | Faculty and Researchers' Publications

1999

Transonic Flutter Computations for a 2D Supercritical Wing

Weber, S.; Jones, K.D.; Ekaterinaris, J.A.; Platzer, M.F.

Weber, S., Jones, K.D., Ekaterinaris, J.A. and Platzer, M.F., "Transonic Flutter Computations for a 2D Supercritical Wing," AIAA Paper No. 99-0798, 37th AIAA Aerospace Sciences Meeting, Reno, Nevada, Jan. 1999.
https://hdl.handle.net/10945/37210

This publication is a work of the U.S. Government as defined in Title 17, United States Code, Section 101. Copyright protection is not available for this work in the United States.

Downloaded from NPS Archive: Calhoun

http://www.nps.edu/library

Calhoun is the Naval Postgraduate School's public access digital repository for research materials and institutional publications created by the NPS community. Calhoun is named for Professor of Mathematics Guy K. Calhoun, NPS's first appointed -- and published -- scholarly author.

Dudley Knox Library / Naval Postgraduate School
411 Dyer Road / 1 University Circle
Monterey, California USA 93943

AIAA−99−0798
TRANSONIC FLUTTER COMPUTATIONS FOR A 2D SUPERCRITICAL WING

S.Weber, K.D.Jones,
J.A.Ekaterinaris and M.F.Platzer
Naval Postgraduate School
Monterey, CA

37th Aerospace Sciences Meeting & Exhibit
January 11−14, 1999 / Reno, NV

For permission to copy or republish, contact the American Institute of Aeronautics and Astronautics 1801 Alexander Bell Drive, Suite 500, Reston, VA 20191

TRANSONIC FLUTTER COMPUTATIONS FOR A 2D SUPERCRITICAL WING

S. Weber[†], K. D. Jones[‡], J. A. Ekaterinaris[⋆] and M. F. Platzer[⋆⋆]

Naval Postgraduate School
Monterey, California

ABSTRACT

A numerical investigation of the transonic two-degree-of-freedom bending/torsion flutter characteristics of the NLR 7301 section is presented using a time domain method. An unsteady, two-dimensional, compressible, thin-layer Navier-Stokes flow-solver is coupled with a two-degree-of-freedom structural model. Furthermore, the Baldwin-Lomax, the Baldwin-Barth and the Spalart-Allmaras turbulence models are implemented, each in conjunction with the transition model of Gostelow et al. The transition onset location can either be predicted with Michel's criterion or specified as an input parameter. Computations of the steady transonic aerodynamic characteristics show good agreement with the experimental results using the Baldwin-Barth or the Spalart-Allmaras model in combination with transition modeling. The aeroelastic computations predict limit-cycle flutter in agreement with the experiment. However, the computed flutter amplitudes are an order of magnitude larger than the measured ones.

NOMENCLATURE

a_∞ = free stream speed of sound
c = chord length
C_l = lift coefficient per unit span
C_m = pitching moment coefficient per unit span
C_p = pressure coefficient
D_h = plunge-damping coefficient
D_α = pitch-damping coefficient
e = total energy per unit volume
f = frequency in Hertz
h = bending displacement (positive downward)
I_α = moment of inertia about x_p per unit span
k = reduced frequency, $\omega c/U_\infty$
k_α = reduced natural pitching frequency, $\omega_\alpha c/U_\infty$
k_h = reduced natural plunging frequency, $\omega_h c/U_\infty$
K_h = spring constant for plunging
K_α = spring constant for pitching
L = lift per unit span
m = mass of the wing per unit span
M = pitching moment per unit span
$\mathbf{M}_\infty$ = free-stream Mach number
Re = Reynolds number
S_α = static moment, $x_\alpha m$
t = time
U_∞ = free-stream speed
u, w = Cartesian velocity components
x = coordinate along chord
x_p = leading edge to elastic axis distance
x_α = elastic axis to center of mass distance
x_t = transition onset location
$\dot{x}|_{wall}$ = velocity component of blade surface
$\dot{y}|_{wall}$ = velocity component of blade surface
y^+ = nondimensional normal wall distance
α = angle of attack
α_0 = spring-neutral angle of attack
δ_h = non-dim. plunge-damping coef., $D_h/(2\sqrt{mK_h})$
δ_α = non-dim. pitch-damping coef., $D_\alpha/(2\sqrt{I_\alpha K_\alpha})$
μ = viscosity
ν = kinematic viscosity
ν_t = turbulent viscosity
ρ = density
ω = circular frequency, $\omega = 2\pi f$
ω_h = undamped natural bending freq., $\sqrt{K_h/m}$
ω_α = undamped natural torsional freq., $\sqrt{K_\alpha/I_\alpha}$
τ = nondimensional time, ta_∞/c
$(\dot{})$ = differentiation with respect to t
$(\,)'$ = differentiation with respect to τ
$|_{wall}$ = quantity on the surface of the blade
$(\,)_\infty$ = free-stream value

INTRODUCTION

It is well known that the flutter speed of typical aircraft wings exhibits a pronounced dip at transonic flight speeds. There is therefore a great need to develop reliable transonic flutter prediction methods ca-

---

[†] Post Doctoral Researcher, Deutsche Forschungsgemeinschaft (DFG)
[‡] Research Assistant Prof., Senior Member, AIAA
[⋆] Senior Research Scientist, NEAR Inc., Associate Fellow, AIAA
[⋆⋆] Professor, Associate Fellow, AIAA

This paper is declared a work of the U.S. Government and is not subject to copyright protection in the United States.

pable of predicting the strong nonlinear/viscous flow phenomena which are encountered in transonic flight. Transonic flutter may also occur on propeller and helicopter blades and in high performance compressor and turbine stages. Especially in turbomachines, the blade chord Reynolds numbers may be quite low and, therefore, improved modeling of the viscous flow effects becomes quite important.

Successful modeling of unsteady transonic flows must not only include the inviscid nonlinear flow features but also the viscous effects caused by the state of the boundary-layer, the shock/boundary-layer interaction, flow-separation and the presence of separation bubbles. For example, Van Dyken et al. (1996) have shown that the boundary-layer transition has a significant effect on the onset of flow separation, even at moderately high Reynolds numbers. Therefore, predictions of transition onset and length are essential to capture flow features, such as separation bubbles and shock/boundary-layer interactions.

Fortunately, with the seemingly unbounded technological advances in computer performance over the last decade, it is now possible to explore these problems with sufficient detail, using aeroelastic solvers. The complex flow physics can be captured with advanced Navier-Stoke analysis which include sophisticated transition modeling and state of the art turbulence models.

The aim of the present work is to numerically investigate the fundamental phenomena which drive transonic flutter of a single airfoil using a thin-layer Navier-Stokes aeroelastic solver. In the present study, the turbulence models of Baldwin and Lomax (1978), of Baldwin and Barth (1990), and of Spalart and Allmaras (1992) are used to model turbulent flow regions. Each turbulence model is coupled with the transition model of Gostelow et al. (1996). Numerical results are compared with experimental measurements of Schewe and Deyhle (1996) and Knipfer et al. (1998) to validate the predictive capability of the code for unsteady transonic flow. Schewe and Deyhle have measured the flutter characteristics of a 2D supercritical wing of the NLR 7301 series in a wind-tunnel. These measurements indicated a transonic dip at a Mach number of 0.77. Limit-cycle oscillations in pitch and plunge were found in the experiment near this Mach number.

The flow solver and the aeroelastic models have been tested and validated extensively in previous studies for a variety of flow conditions. For example, the flow solver and the turbulence models have been tested for subsonic flow by Sanz and Platzer (1998), Ekaterinaris and Menter (1994), Ekaterinaris et al. (1998) and for transonic flow by Ekaterinaris et al. (1994). The aeroelastic model has been implemented and tested by Jones and Platzer (1998) for inviscid flow calculations.

The ability of the numerical solution to capture shock/boundary-layer interactions in steady-state transonic flow is first demonstrated and the effect of transition modeling for these flow conditions is shown. Numerical solutions for an airfoil free to oscillate in one- or two-degrees-of-freedom in transonic flow are obtained.

NUMERICAL METHODS

Aeroelastic behavior of a blade or a wing can be predicted by solving the aerodynamic flow in combination with the structural dynamics. The flow solver and the method used to compute the structural response to the aerodynamic flow field are presented in the following sections.

AERODYNAMICS

The unsteady, compressible, two-dimensional, thin-layer Navier-Stokes equations in the strong conservation-law form and curvilinear coordinate system (ξ, ζ) are

$$\partial_t \hat{\mathbf{Q}} + \partial_\xi \hat{\mathbf{F}} + \partial_\zeta \hat{\mathbf{G}} = Re^{-1} \partial_\zeta \hat{\mathbf{S}} \tag{1}$$

where $\hat{\mathbf{Q}}$ is the vector of conservative variables,

$$\hat{\mathbf{Q}} = \frac{1}{J} \begin{Bmatrix} \rho \\ \rho u \\ \rho w \\ e \end{Bmatrix}, \tag{2}$$

$\hat{\mathbf{F}}$ and $\hat{\mathbf{G}}$ are the inviscid flux vectors,

$$\hat{\mathbf{F}} = \frac{1}{J} \begin{Bmatrix} \rho U \\ \rho u U + \xi_x p \\ \rho w U + \xi_z p \\ (e+p)U - \xi_t p \end{Bmatrix}, \tag{3}$$

$$\hat{\mathbf{G}} = \frac{1}{J} \begin{Bmatrix} \rho W \\ \rho u W + \zeta_x p \\ \rho w W + \zeta_z p \\ (e+p)W - \zeta_t p \end{Bmatrix} \tag{4}$$

and $\hat{\mathbf{S}}$ is the thin-layer approximation of the viscous fluxes in the ζ direction (normal to the airfoil surface),

$$\hat{\mathbf{S}} = \frac{1}{J} \begin{Bmatrix} 0 \\ \mu m_1 u_\zeta + (\mu/3) m_2 \zeta_x \\ \mu m_1 w_\zeta + (\mu/3) m_2 \zeta_z \\ \mu m_1 m_3 + (\mu/3) m_2 m_4 \end{Bmatrix}, \tag{5}$$

where

$$m_1 = \zeta_x^2 + \zeta_z^2, \tag{6}$$

$$m_2 = \zeta_x u_\zeta + \zeta_z w_\zeta, \tag{7}$$

$$m_3 = (u^2 + w^2)/2 + (\gamma - 1)^{-1} Pr^{-1} \partial_\zeta (a^2) \tag{8}$$

and

$$m_4 = \zeta_x u + \zeta_z w. \tag{9}$$

The terms U and W are the contravariant velocity components given by

$$U = u\xi_x + w\xi_z + \xi_t \tag{10}$$

and

$$W = u\zeta_x + w\zeta_z + \zeta_t \tag{11}$$

and J is the metric Jacobian, where

$$J^{-1} = x_\xi z_\zeta - x_\zeta z_\xi \ . \tag{12}$$

Pressure is related to the other variables through the equation of state for an ideal gas

$$p = (\gamma - 1)\Big[e - \rho(u^2 + w^2)/2\Big] \ . \tag{13}$$

Eqs. (1-13) are nondimensionalized using c as the reference length, a_∞ as the reference speed, c/a_∞ as the reference time, ρ_∞ as the reference density and $\rho_\infty a_\infty^2$ as the reference energy.

For Euler solutions, the viscous terms on the RHS are set to zero, and flow-tangency boundary conditions are used at the surface. For Navier-Stokes solutions, the no-slip condition is applied. Density and pressure are extrapolated to the wall for both Euler and Navier-Stokes solutions.

For unsteady airfoil motions, the flow-tangency and no-slip conditions are modified to include the local motion of the surface which also contributes to the pressure on the surface. Therefore, the momentum equation normal to the surface (ζ direction) is solved to predict the pressure for a viscous flow more accurately

$$\begin{aligned}\partial_\zeta p|_{wall} = & -\frac{1}{\nabla^2\zeta}\left[\rho\ \partial_t \left\{ \begin{array}{c} \dot{x}|_{wall} \\ \dot{y}|_{wall} \end{array} \right\} \cdot \nabla\zeta \right. \\ & \left. +\ \partial_\zeta p|_{wall} \nabla\xi \cdot \nabla\zeta \right] ,\end{aligned} \tag{14}$$

where $\dot{x}|_{wall}$ and $\dot{y}|_{wall}$ are the components of the blade velocity. Furthermore, by assuming that the grid is orthogonal at the surface $\nabla\xi \cdot \nabla\zeta = 0$. If the blade is stationary, the normal pressure gradient vanishes in agreement with boundary-layer theory.

The numerical algorithm, developed by Ekaterinaris and Menter (1994), performs time integration with the implicit, factorized, iterative scheme of Rai and Chakravarthy (1988) given by Eq. (15). In Eq. (15), $h_\xi = \Delta\tau/\Delta\xi$ etc., $\hat{A}^\pm = \partial\hat{F}/\partial\hat{Q}$ etc. are the flux Jacobian matrices and ∇, Δ and δ are the forward, backward and central difference operators, respectively. The quantities $\hat{F}_{i+1/2,k}$, $\hat{G}_{i,k+1/2}$ and $\hat{S}_{i,k+1/2}$ are numerical fluxes. The superscript $(\cdot)^n$ denotes the time step, and the superscript $(\cdot)^p$ refers to Newton subiterations within each time step.

$$\begin{aligned}&\Big[I + h_\xi\Big(\nabla_\xi \hat{A}^+_{i,k} + \Delta_\xi \hat{A}^-_{i,k}\Big)\Big]^p \\ &\quad \times \Big[I + h_\zeta\Big(\nabla_\zeta \hat{B}^+_{i,k} + \Delta_\zeta \hat{B}^-_{i,k} - Re^{-1}\delta_\zeta \hat{M}_{i,k}\Big)\Big]^p \\ &\quad \times \Big(\hat{Q}^{p+1}_{i,k} - \hat{Q}^p_{i,k}\Big) \\ &= -\Big[\Big(\hat{Q}^p_{i,k} - \hat{Q}^n_{i,k}\Big) \\ &\quad + h_\xi\Big(\hat{F}^p_{i+1/2,k} - \hat{F}^p_{i-1/2,k}\Big) \\ &\quad + h_\zeta\Big(\hat{G}^p_{i,k+1/2} - \hat{G}^p_{i,k-1/2}\Big) \\ &\quad - Re^{-1}h_\zeta\Big(\hat{S}^p_{i,k+1/2} - \hat{S}^p_{i,k-1/2}\Big)\Big] \ .\end{aligned} \tag{15}$$

The inviscid fluxes, $\hat{F}$ and $\hat{G}$, are evaluated using Osher's third-order upwind-biased scheme (Osher and Chakravarthy, 1985 and Chakravarthy and Osher, 1983). Linearization of the left-hand side of Eq. (15) is performed by evaluating the flux Jacobian matrices, A and B, with the Steger-Warming flux-vector splitting (Steger and Warming, 1981). The viscous fluxes are computed with second-order central differences. Furthermore, a standard minmod TVD scheme (Osher and Chakravarthy, 1985) is used to eliminate numerical oscillations at shocks developed at transonic Mach numbers.

Time accuracy is improved by performing Newton subiterations to convergence at each step. These subiterations minimize the linearization and factorization errors and help drive the left-hand side of Eq. (15) to zero within each physical time step. Numerical experiments have shown that larger CFL numbers (i.e., a larger time step) could be used if the number of Newton iterations was increased. The optimum seemed to depend on the grid density and flow conditions, but the best computational performance appears to occur with 4 to 5 sub-iterations on coarse grids (Euler simulations), and 2 to 3 sub-iterations on fine grids (Navier-Stokes simulations). The Navier-Stokes solver has been tested extensively in a variety of unsteady subsonic and transonic studies such as Ekaterinaris et al. (1994).

The turbulence modeling is based either on the standard algebraic model of Baldwin and Lomax (1978) (BL) or the one equation models of Baldwin and Barth (1990) (BB) or Spalart and Allmaras (1992)(SA). The eddy-viscosity obtained from the models is used for the computation of the fully turbulent region and for the evaluation of an effective eddy viscosity in the transitional flow region as is explained next.

TRANSITION MODELING

The transition modeling for all turbulence models follows Sanz and Platzer (1998). In this publication the model of Gostelow et al. (1996) was introduced which permits the calculation of the transition length as a function of pressure gradient and free-stream turbulence level. This method continuously adjusts the turbulent spot growth in response to changes of the local pressure gradient.

The intermittency function in the transitional region is given by

$$\gamma(x) = 1 - \exp\left[-n\int_{x_t}^{x_i}\frac{\sigma}{\tan\alpha}\left(\frac{dx}{U}\right)\int_{x_t}^{x_i}\tan\alpha dx\right], \quad (16)$$

where the correlations for the variation of the spot propagation parameter σ and the spot spreading half angle ϵ as functions of the pressure gradient parameter λ_θ are

$$\epsilon = 4 + \frac{22.14}{0.79 + 2.72\exp(47.63\lambda_\theta)} \quad (17)$$

and

$$\sigma = 0.03 + \frac{0.37}{0.48 + 3.0\exp(52.9\lambda_\theta)} \ . \quad (18)$$

Here $\lambda_\theta = (\theta^2/\nu)/(dU/dx)$ with the boundary-layer momentum thickness, θ, and the outer-edge velocity, U. The spot generation rate, n, is inferred from the dimensionless breakdown-rate parameter, N, where

$$N = n\sigma\lambda_{\theta_t}^3/\nu \ , \quad (19)$$

$$N = 0.86\times10^{-3}\exp(2.134\lambda_{\theta_t}\ln(q_t) - 59.23\lambda_{\theta_t} - 0.564\ln(q_t)), \text{ for } \lambda_{\theta_t}\le 0 \quad (20)$$

and

$$N = N(\lambda_\theta = 0)\times\exp(-10\sqrt{\lambda_{\theta_t}}), \text{ for } \lambda_{\theta_t} > 0 \ , \quad (21)$$

and where q_t denotes the free-stream turbulence.

The spot-propagation-rate and the spot spreading half-angle asymptotically approach a maximum value for high negative values of λ_θ, but n is allowed to increase to infinity for high negative values of λ_{θ_t}, where λ_{θ_t} is the pressure gradient at the transition onset location, x_t. The value of the intermittency parameter, $\gamma(x)$, is zero for $x \le x_t$, and increases downstream from the transition point, asymptotically to a maximum value of unity, which corresponds to fully-turbulent flow. An effective eddy-viscosity for the transitional region is obtained by scaling the turbulent eddy-viscosity computed by $\gamma(x)$, i.e. $\mu_{trans} = \gamma(x)\mu_{turb}$.

Sanz and Platzer (1998) have used the Gostelow model, originally developed for attached flow, for the prediction of laminar separation bubbles by using the spot-generation rate as a second adjustable parameter along with the location of transition onset. They investigated the influence of the spot-generation rate on the separation bubble by either limiting the breakdown-rate parameter to 1.0, which forces instantaneous transition, or by assuming the value for a zero pressure-gradient. In the present study a breakdown-rate parameter of 1.0 was chosen and the transition onset was either predicted by the Michel criterion (Cebeci and Bradshaw, 1977) or by specification as an input parameter.

STRUCTURAL DYNAMICS

Structural modeling is facilitated using a two-degree-of-freedom spring/mass/damper system (Fig. 1) to simulate the bending and twisting of a wing.

The equations governing this motion are

$$m\ddot{h} + S_\alpha\ddot{\alpha} + D_h\dot{h} + m\omega_h^2 h = -L \quad (22)$$

and

$$S_\alpha\ddot{h} + I_\alpha\ddot{\alpha} + D_\alpha\dot{\alpha} + I_\alpha\omega^2_{\alpha-\alpha_0}\alpha = M \ , \quad (23)$$

where the dots denote differentiation with respect to time.

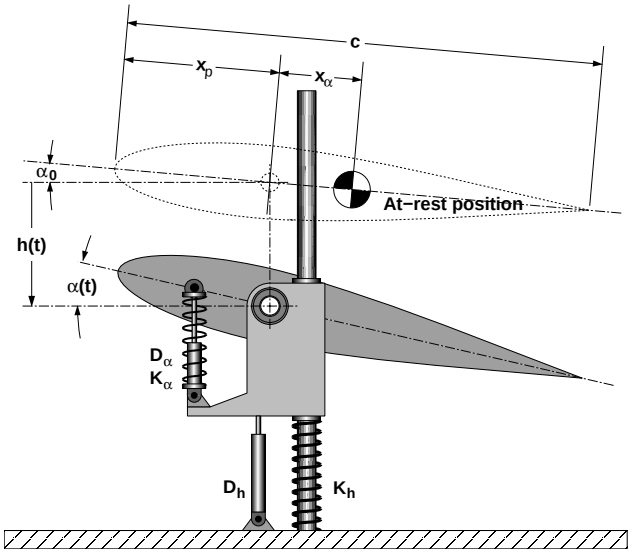

Fig. 1. Schematic of the spring/mass/damper system.

Equations (22, 23) are nondimensionalized using reference length c, reference velocity a_∞, reference mass $\rho_\infty\pi(c/2)^2$, and reference inertia $\rho_\infty\pi(c/2)^2c^2$.

Rewriting Eqs. (22) and (23) in matrix notation one obtains

$$[\mathbf{M}]\{X\}'' + [\mathbf{D}]\{X\}' + [\mathbf{K}]\{X\} = \{F\} \tag{24}$$

where

$$[\mathbf{M}] = \begin{bmatrix} m & S_\alpha \\ S_\alpha & I_\alpha \end{bmatrix}, \; [\mathbf{D}] = \begin{bmatrix} 2\delta_h m k_h & 0 \\ 0 & 2\delta_\alpha I_\alpha k_\alpha \end{bmatrix},$$

$$[\mathbf{K}] = \begin{bmatrix} m k_h^2 & 0 \\ 0 & I_\alpha k_\alpha^2 \end{bmatrix}, \; \{X\} = \begin{Bmatrix} h \\ \alpha - \alpha_0 \end{Bmatrix}$$

and

$$\{F\} = \frac{2}{\pi}\mathbf{M}_\infty^2 \begin{Bmatrix} -C_l \\ C_m \end{Bmatrix},$$

where the primes denote differentiation with respect to nondimensional time, $\tau = ta_\infty/c$, and the other parameters (i.e., m, I_α,...) are now non-dimensional. Note that k_h and k_α appearing in the matrices $[\mathbf{K}]$ and $[\mathbf{D}]$ are reduced natural frequencies based on the free-stream speed of sound, as opposed to the conventional form as presented in the nomenclature. However, in the interest of clarity, presented results utilize the conventional definition, based on free-stream velocity.

Equation (24) is a system of two, coupled, second-order, ordinary differential equations. Coupling is obtained through the terms containing S_α and the dependence of C_l and C_m on h and α. The system is nonlinear through the nonlinearity of C_l and C_m. Linearization is introduced by treating C_l and C_m as constants, computed from the previous time-step of the flow solution.

Simulations with a single-degree-of-freedom may be performed by setting $S_\alpha = 0$ and either $m = \infty$ and $\omega_h = 0$ or $I_\alpha = \infty$ and $\omega_\alpha = 0$ for pitching-only or plunging-only motions, respectively.

Equation (24) is advanced in time by inverting the system, yielding

$$\begin{aligned} \{X\}'' = & [\mathbf{M}]^{-1}\{F\} \\ & - [\mathbf{M}]^{-1}[\mathbf{K}]\{X\} - [\mathbf{M}]^{-1}[\mathbf{D}]\{X\}' , \end{aligned} \tag{25}$$

then rewriting the result as a system of two, coupled, first-order equations

$$\begin{aligned} \{X\}' &= \{Y\} \\ \{Y\}' &= [\mathbf{M}]^{-1}\{F\} \\ & - [\mathbf{M}]^{-1}[\mathbf{k}]\{X\} - [\mathbf{M}]^{-1}[\mathbf{D}]\{Y\} , \end{aligned} \tag{26}$$

and, finally, time integration is performed using a 1st-order accurate explicit Euler scheme. Higher-order methods were tested (eg. 4th-Order Runge-Kutta), but the stability requirements of the Navier-Stokes code are such that time-steps are small enough to achieve sufficient accuracy with the 1st-order Euler explicit time integration scheme.

The accuracy of the structural integration was evaluated by removing the aerodynamic influence from the problem, and releasing the airfoil with initial disturbances in α and/or h. The kinetic and potential energy of the system was then computed as the airfoil oscillated in time. For the undamped system, the energy should remain constant for all time.

The 1st-order Euler integration predicted a small oscillation, such that the energy was periodic, with an amplitude of roughly 0.3 percent of the total energy when 1000 steps per cycle were used. The energy fluctuation diminished linearly with the step-size. The Navier-Stokes solutions included in the paper typically require between 1500 and 3500 steps per cycle, so this energy fluctuation was deemed acceptable.

RESULTS

For the present study, simulations were performed for the measurements obtained at experimental flow conditions of free-stream Mach number of 0.768 at an angle of attack of 1.28 degrees (Knipfer et al., 1998, data for measurement no. 77). For these conditions, limit-cycle oscillations in two-degrees-of-freedom were found in the experiment. The experimental Reynolds number (based on chord length) was 1.727×10^6 based on a chord length of $0.3m$ for the NLR7301 airfoil model.

In the experiment, the square shaped wind-tunnel test-section had an area of $1m^2$, and the $0.3m$ chord model was installed in the center. Due to this relatively large chord length Knipfer et al. (1998) corrected for steady wind-tunnel interference effects at subsonic speeds. However, no corrections for steady transonic and oscillatory interference effects were attempted. Therefore, in this paper both the free-stream Mach number (M_c) and the angle of attack (α_c) were corrected until a reasonable agreement with the measured time-averaged surface pressure distribution was achieved.

All steady and unsteady viscous computations were carried out on a C-type 221 × 91 point grid which was generated from the original NLR7301 airfoil surface data taken from the *University of Illinois, Champagne-Urbana, Department of Aeronautical and Astronautical Engineering, Airfoil Coordinates Database (www.uiuc.edu/ph/www/m-selig/ads/coord_database.html).*

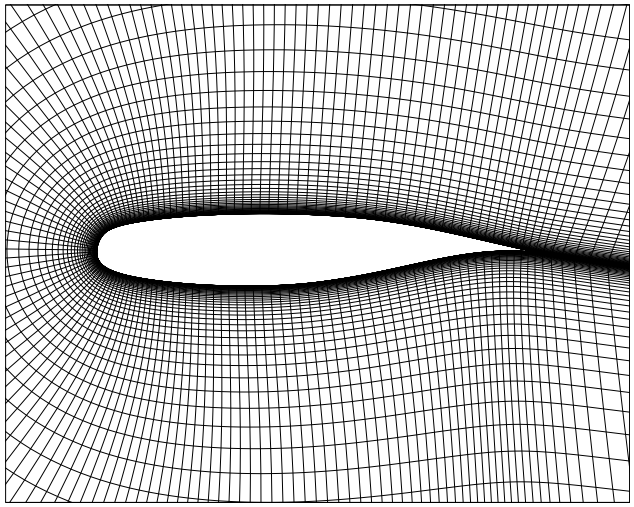

Fig. 2. C-type grid for the NLR 7301 airfoil.

A preliminary grid-sensitivity investigation was performed for steady state solutions by varying initial wall spacing, grid density in both directions, and outer boundary location. As a result, a grid with an initial wall spacing of 2×10^{-5}, which yields $y^+ < 1.0$, with 40 grid points in the wake and with the farfield boundary extended by 20 chord lengths from the surface was chosen. The grid is shown in Fig. 2.

STEADY STATE COMPUTATIONS

At the beginning of the study, Euler computations were performed on an C-type grid with 201 × 41 points. However, even with a corrected free-stream Mach number and a corrected angle of attack the agreement between the computed and the measured results was poor. Therefore, the free-stream Mach number and angle of attack were corrected by performing viscous computations. The computed inviscid pressure distribution for the same flow conditions which yield best agreement with the experiment with viscous computations is shown in Fig. 3. This indicates that viscous effects are important, as the strength and location of the shock on the suction side are clearly missed by the inviscid solver.

A closer agreement with the experimental data was achieved by viscous computations with the Baldwin-Lomax turbulence model assuming fully turbulent flow (see Fig. 4). The best agreement was found for $M_c = 0.753$ and $\alpha_c = -0.08$ degrees. The fully turbulent result could be improved by taking transition into account. Because no data of the transition onset location where available from the experiment, the transition-onset location was computed using the Michel criterion.

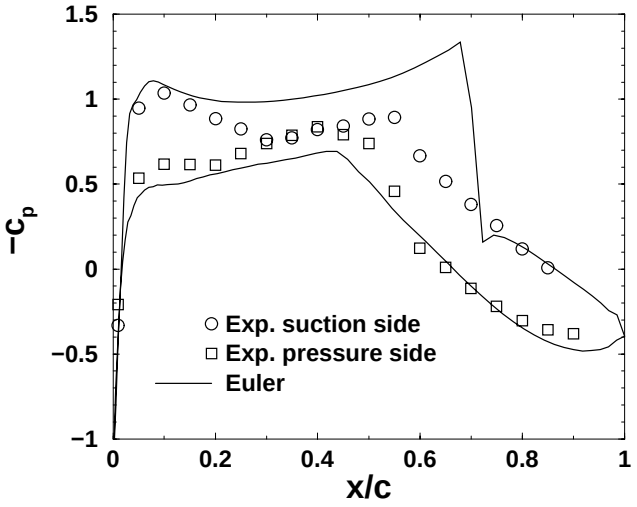

Fig. 3. Pressure dist.; $M_c = 0.753$, $\alpha_c = -0.08°$.

Michel's criterion predicted the transition onset at almost 60% chord on the suction side, leading to a pressure distribution on the suction side similar to the pressure distribution computed by the Euler code.

Michel's criterion predicted the onset location at 19% chord on the pressure side which improved the pressure distribution on the pressure side slightly. It was found that moving the transition onset location further downstream could improve the steady-state result even more. Computations without transition and with forced transition on the suction side at 3% and on the pressure side at 44% chord length are shown in Fig. 4.

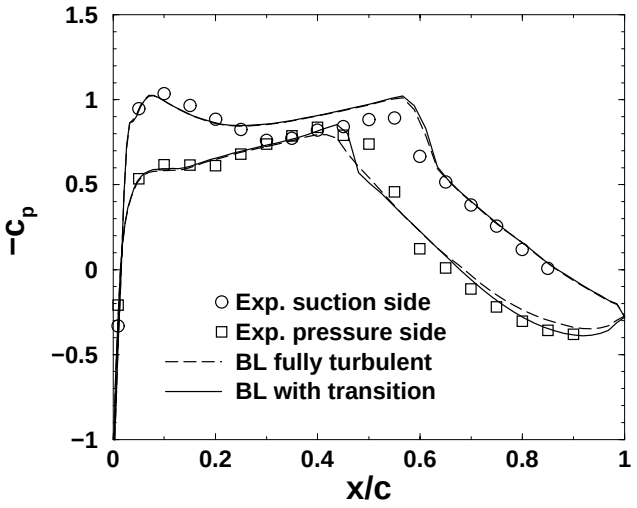

Fig. 4. Pressure dist.; $M_c = 0.753$, $\alpha_c = -0.08°$.

Steady-state computations could be greatly accelerated by using a local-time-stepping scheme, with no measurable difference, in terms of accuracy, to the results of the time-accurate time-stepping scheme. Typ-

ically 3000 time steps were required to converge at a Courant number of 30.

The BB and SA turbulence models provided marginally better agreement with experiment results than the BL model. The computed pressure distributions for the three models are compared with the experimental data in Fig. 5. The BB and SA models provide nearly identical pressure distributions for the steady solution. Compared with the BL solution for fully turbulent flow, the pressure distributions computed by the BB and SA models on the suction side are slightly worse in the range between 4% and 20% chord length, but the agreement in front of the shock is better. On the pressure side, the pressure distribution is in much better agreement with the experiment between the leading edge and 45% chord length, leading to a stronger shock than predicted by the BL model. From 70% chord length to the trailing edge the BL result is closer to the measurements.

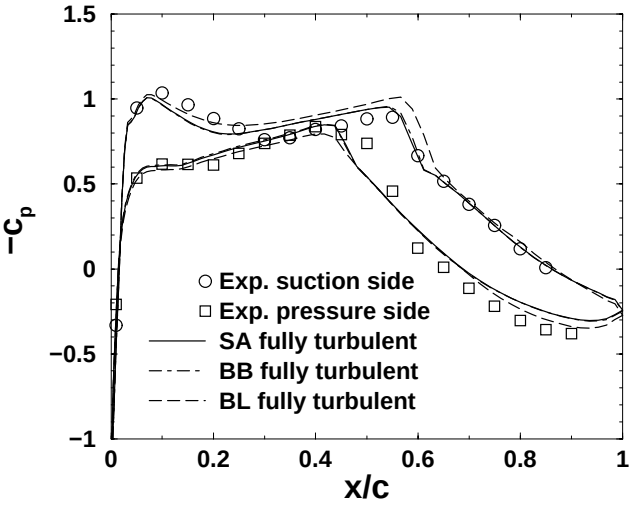

Fig. 5. Pressure dist.; $M_c = 0.753$, $\alpha_c = -0.08°$.

Taking transition into account improved the steady-state results slightly, as shown in Fig. 6. Again the BB and the SA turbulence models yield almost the same result. Similar to the experience with the BL model, the use of Michel's criterion on the suction side led to an unrealistic transition onset location. Therefore, transition onset on the suction side was enforced at 3% chord length. On the pressure side, Michel's criterion predicted a reasonable onset location at 44% chord length which improved the steady-state result near the trailing edge.

In Figs. 7 and 8 the boundary-layer profiles of the suction and the pressure side are compared for computations which included transition. All computations predicted no laminar separation bubbles. Separation was found on the suction side close to the trailing edge for all turbulence models. The location of separation onset was computed at 83% chord length with the BL and the BB model, and at 90% chord length with the SA model. A small separation bubble in th shock region due to shock/boundary-layer interaction was found only for the computation with the BL model.

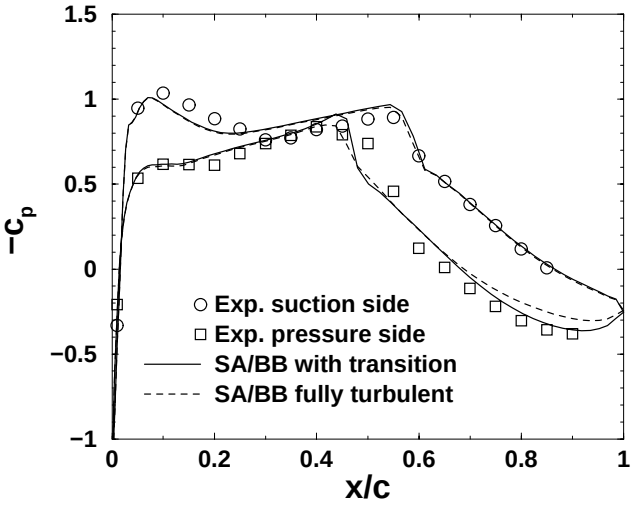

Fig. 6. Pressure dist.; $M_c = 0.753$, $\alpha_c = -0.08°$.

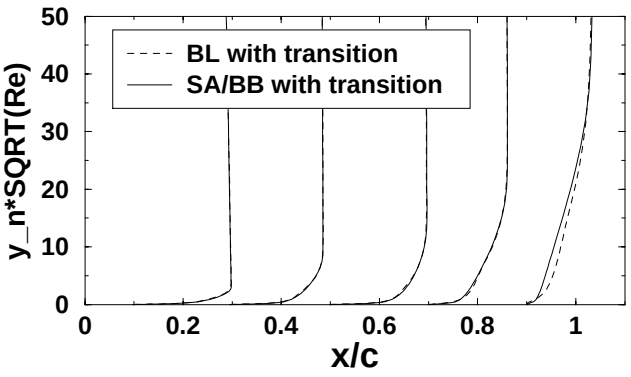

Fig. 7. Boundary-layer profiles on the suction side.

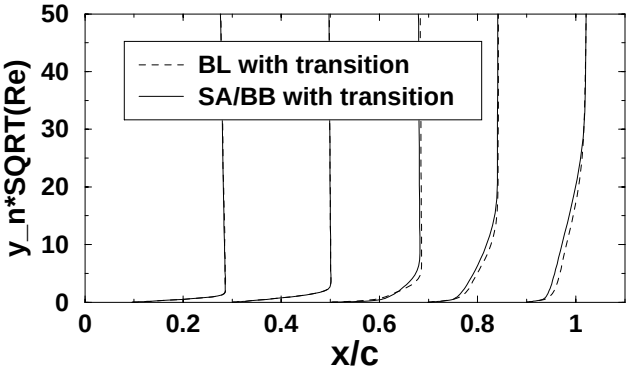

Fig. 8. Boundary-layer profiles on the pressure side.

All computations with the BB and SA turbulence model had to be performed time-accurately. A Courant number of 1000 was used and full convergence was achieved after 6000 time steps.

FLUTTER COMPUTATIONS

Unsteady computations were then performed using the previously presented steady-state results as starting solutions. For the experimental test case no. 77 (Knipfer et al, 1998) with a free-stream Mach number of $M = 0.768$ (close to the transonic dip), limit-cycle oscillations in pitch and plunge were found. The experiment was conducted at a total pressure of 0.45 bar and a dynamic pressure of 0.126 bar. A time-averaged angle of attack of $\bar{\alpha} = 1.28$ degrees was measured for an angle of attack at wind-off condition of $\alpha_0 = 1.91$ degrees which is equivalent to the spring-neutral angle of attack, α_0, in the numerical simulation.

The same free-stream Mach number and the angle of attack corrections applied for the steady-state computations ($M = 0.753$, $\alpha = -0.08$ degrees , were used in unsteady computations. The spring-neutral angle of attack, α_{0c}, was changed until the calculated time-averaged angle of attack was close to the corrected angle of attack of the steady-state computations ($\alpha = -0.08$ degrees).

The initial energy needed to disturb the airfoil from its rest or *steady-state* position was derived from the static-imbalance of the aerodynamic moment and the moment of the spring. The nondimensional structural parameters of the experiment used for the unsteady computations are summarized in Table 1.

Table 1: Structural parameters

$x_p =$	0.2500	$k_\alpha =$	0.3280
$x_\alpha =$	0.0485	$k_h =$	0.2510
$m =$	992.00	$\delta_\alpha =$	0.0041
$I_\alpha =$	35.600	$\delta_h =$	0.0073

The first series of flutter computations were performed assuming fully turbulent flow. The starting solutions for each turbulence model were the same as given in Fig. 5. It turned out that for all turbulence models the NLR 7301 airfoil began to flutter in two-degree-of-freedom. Limit cycle oscillations were predicted for all turbulence models. As an example Fig. 9 shows the time history of the pitching amplitude which was obtained from a fully turbulent computation with the SA turbulence model.

All computations predicted flutter frequencies approximately 1.5% higher and inter-modal phase angles approximately 7% lower than the experiment. The phase angle was estimated from the phase of the fundamental frequencies of pitch and plunge predicted by DFT-analysis of the last 10 cycles. Despite this agreement, for all turbulence models, the computed pitching and plunging amplitude of the limit cycle were off by an order of magnitude or more. Computations with and without structural damping showed that damping affects neither the flutter frequency nor the phase angle but decreased the pitch amplitude by 9% and the plunge amplitude by 7%.

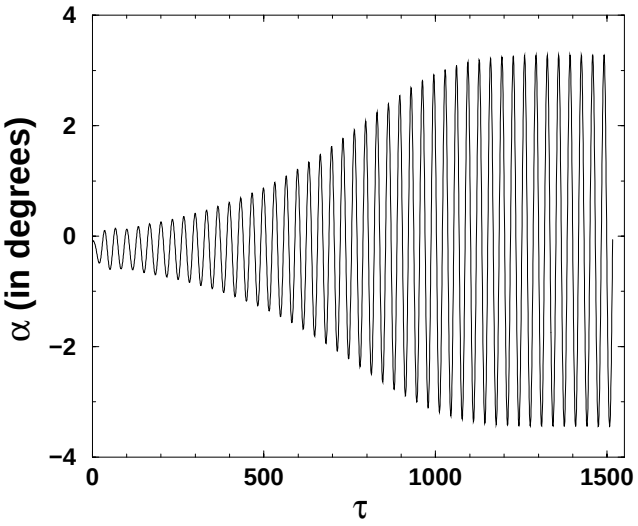

Fig. 9. SA fully turbulent.

The influence of transition on the flutter behavior was studied in a second series of computations. For this series the Spalart-Allmaras model was used because it allowed the biggest time-steps. Unsteady runs were performed starting from the solution given in Fig. 6. Because of lack of measured data, transition on the suction side was forced at 3% chord length and on the pressure side Michel's criterion was applied. As a result the transition location was recalculated during flutter. Again limit cycle flutter in two-degree-of-freedom was predicted. In Fig. 10, the time history of the pitching amplitude shows that the limit-cycle amplitude was higher and didn't stay as constant as the fully turbulent computations.

An inter-modal phase angle of approximately 170 degrees was predicted (see Fig. 11). In Figs. 12 and 13 the pitching moment and lift coefficient time history are shown. The dots in Figs. 11-13 indicate the points through an oscillation cycle that correspond to the Mach-contour plots in Figs. 14a-l. Some of the dots are labeled for easier comparison. In Figs. 14a-l, the dotted or broken line indicates the location of the sonic line.

While the time history of the lift coefficient is al-

most smooth and harmonic, the time variation of the pitching-moment coefficient clearly shows the nonlinear response of the flow field to the limit cycle flutter motion. Looking at the Mach-contour plots, one can see that the plateau in the moment coefficient time history between (a) and (d) occurs when the airfoil is pitching up and plunging down, which corresponds to the portion of the cycle where the effective angle of attack is the highest. During this period the shock on the suction side becomes stronger and moves upstream causing a shock induced separation.

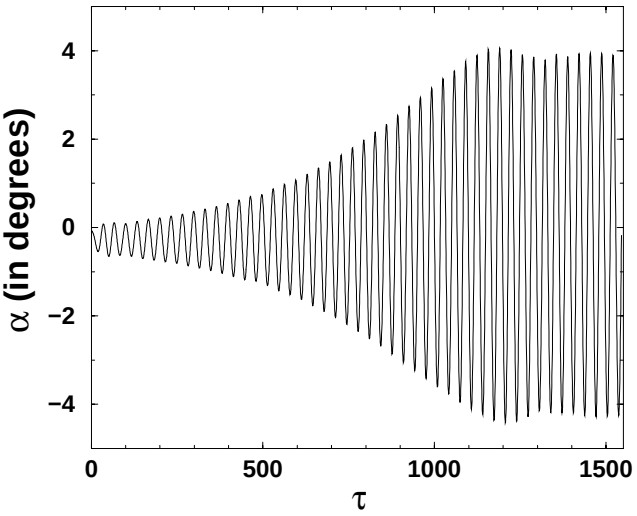

Fig. 10. SA with transition.

Once the turning point of the pitch motion is reached the plateau ends and a smooth moment coefficient variation between (d) and (g) is predicted. The highest pitch-moment coefficient is found between (g) and (h). After the highest moment coefficient is reached, a steep decrease of the moment coefficient is predicted between (h) and (j) during which the airfoil is pitching down and plunging up, corresponding to a low effective angle of attack. Once the turning point for the pitch and plunge motion (j) is reached, the curve shows a smooth development between (j) and (l). Looking at one cycle, the dominating nonlinear flow effects occur between (a) and (d) and (h) and (j). During these time periods the airfoil plunging and pitching speed is decelerating, and the magnitude of the effective angle of attack is the highest.

Although inclusion of transition improved the prediction of the phase difference between pitch and plunge, it did not affect the over-prediction of the amplitudes. On the contrary, higher amplitudes were predicted. All the unsteady computations showed that even if the computed time-averaged angle of attack differed from the steady-state angle of attack by 0.1 degree, it had no significant influence on the overall flutter behavior.

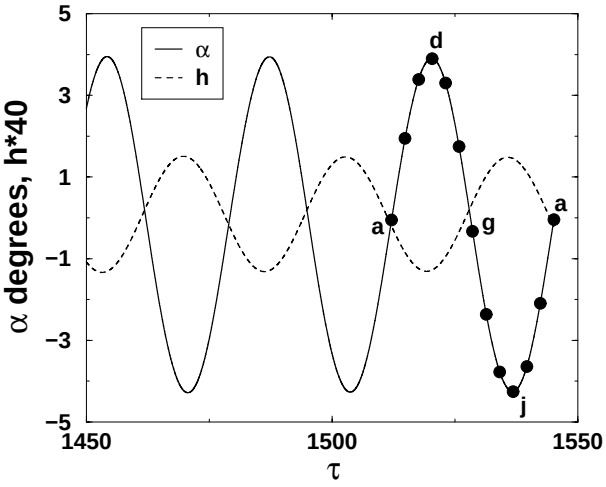

Fig. 11. SA; limit cycle in two-degree-of-freedom.

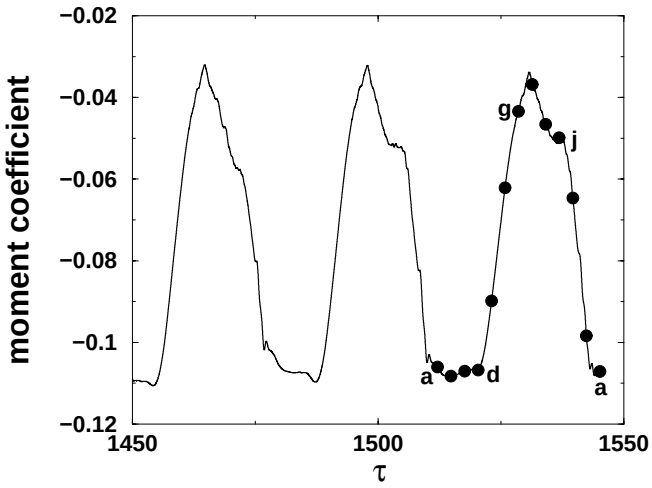

Fig. 12. SA computed moment coefficient.

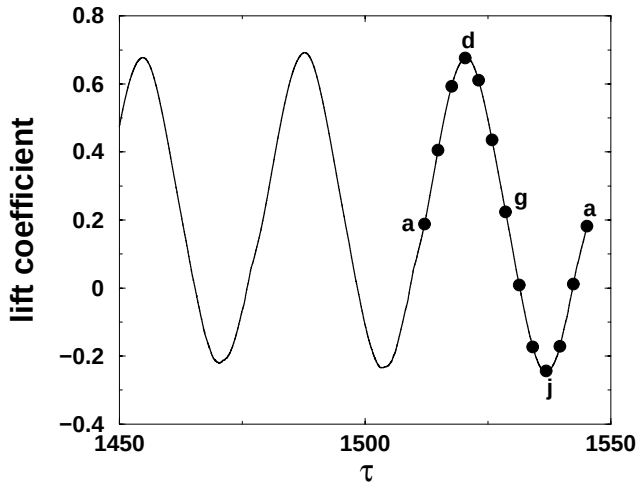

Fig. 13. SA computed lift coefficient.

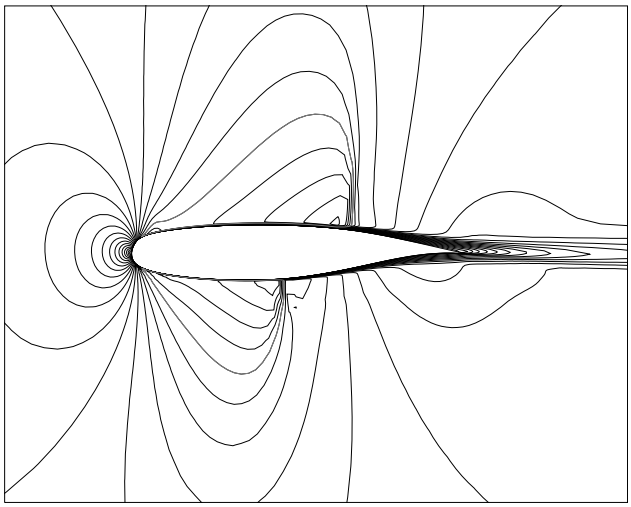

Fig. 14a. $\alpha = -0.05°$ up, $h = -0.005$ down.

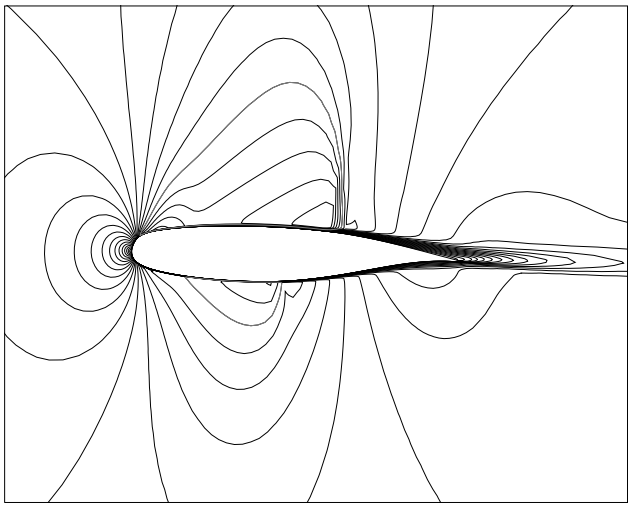

Fig. 14b. $\alpha = 1.95°$ up, $h = -0.021$ down.

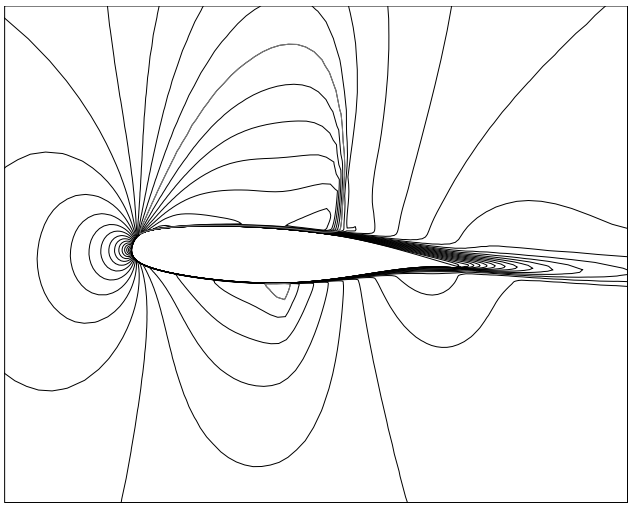

Fig. 14c. $\alpha = 3.40°$ up, $h = -0.030$ down.

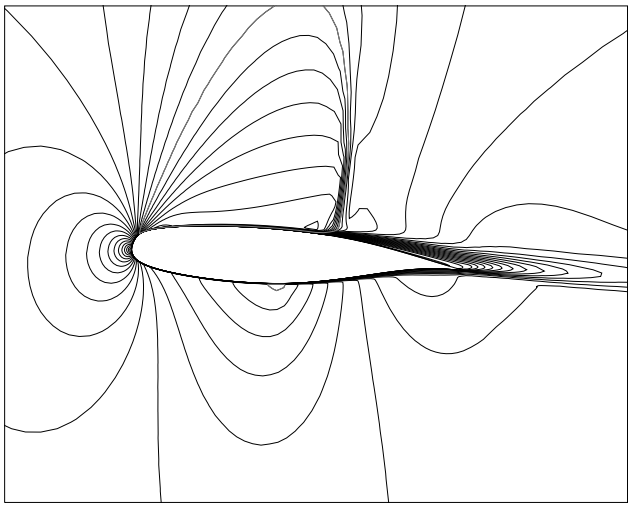

Fig. 14d. $\alpha = 3.90°$ up, $h = -0.032$ up.

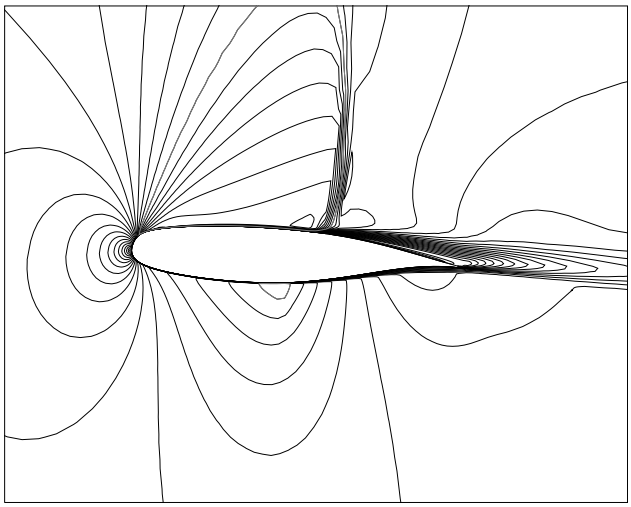

Fig. 14e. $\alpha = 3.30°$ down, $h = -0.024$ up.

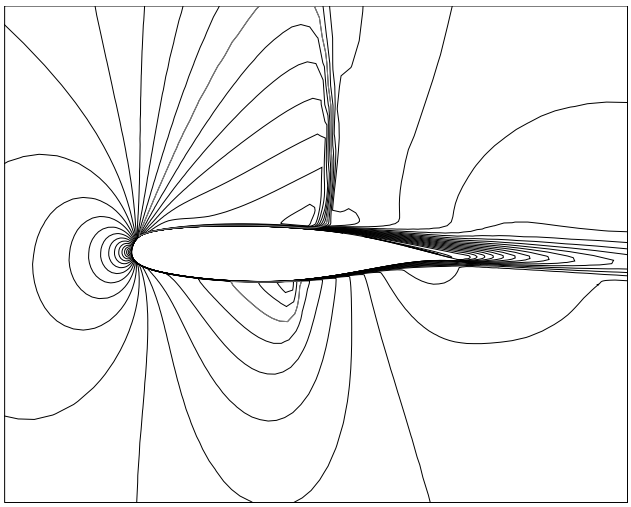

Fig. 14f. $\alpha = 1.75°$ down, $h = -0.009$ up.

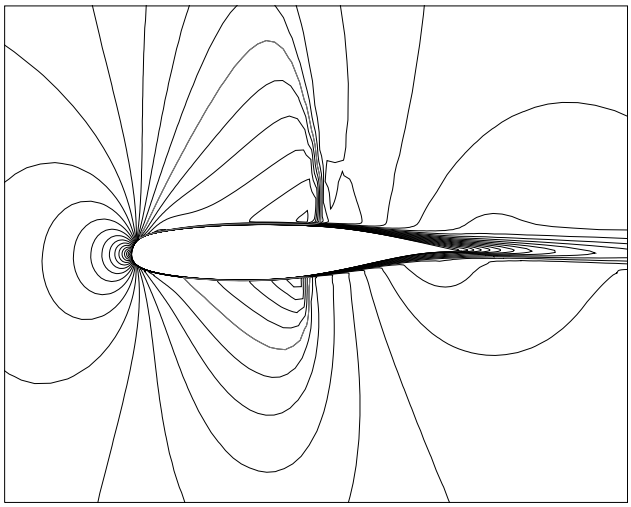

Fig. 14g. $\alpha = -0.33°$ down, $h = 0.009$ up.

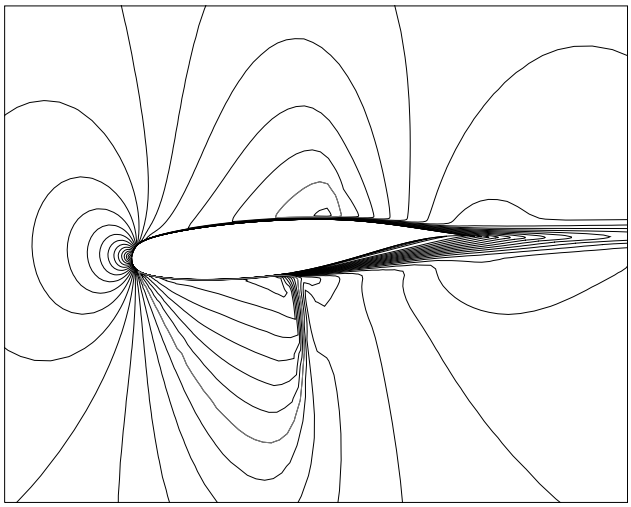

Fig. 14j. $\alpha = -4.25°$ down, $h = 0.036$ down.

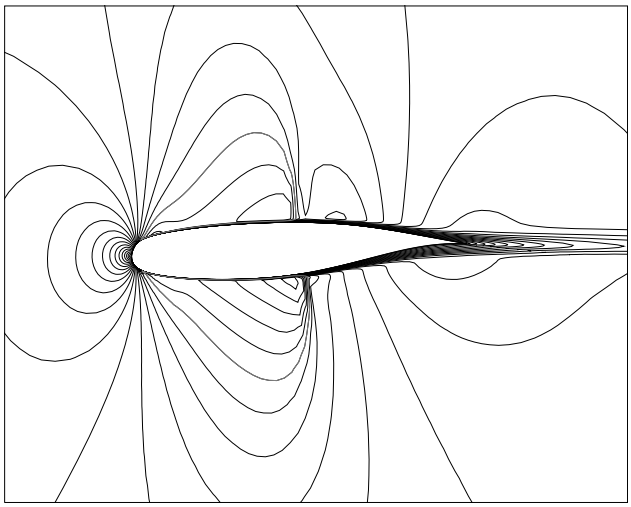

Fig. 14h. $\alpha = -2.36°$ down, $h = 0.026$ up.

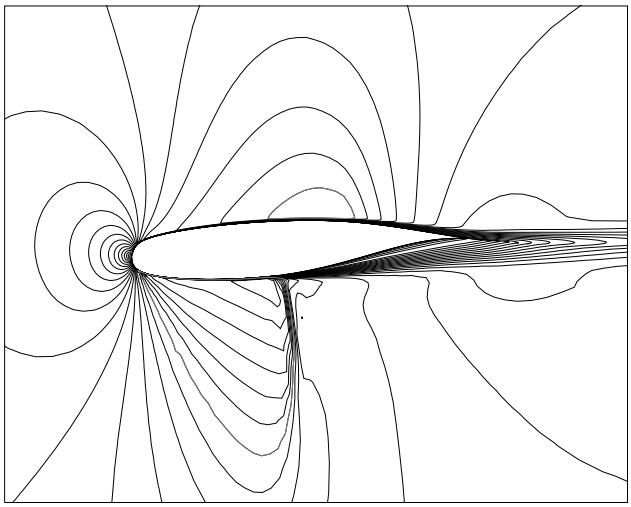

Fig. 14k. $\alpha = -3.64°$ up, $h = 0.028$ down.

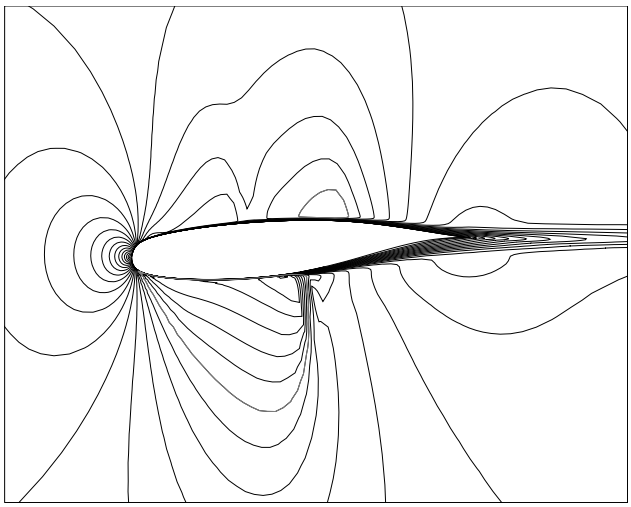

Fig. 14i. $\alpha = -3.78°$ down, $h = 0.035$ up.

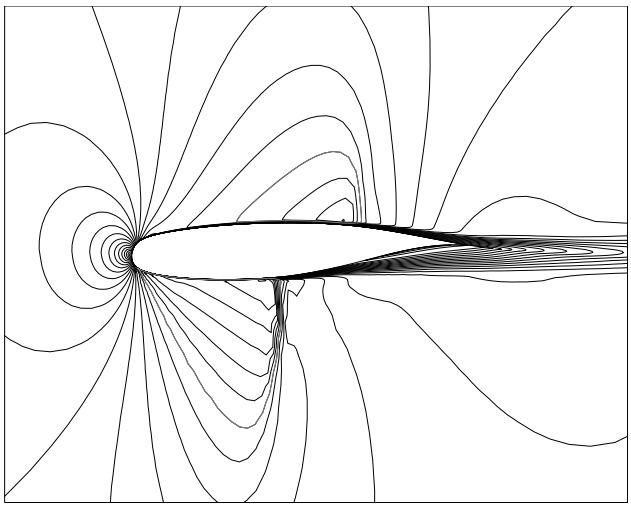

Fig. 14l. $\alpha = -2.10°$ up, $h = 0.0128$ down.

The results of the transitional flutter computation are given in detail in the following tables. The free-stream Mach number, angle of attack, and spring-neutral angle of attack are given in Table 2. For comparison, the uncorrected values of the experiment are given in the first row of the table. The corrected values, taking into account wind-tunnel effects, are given in the second row. Flutter frequency, phase, amplitudes $\hat{\alpha}$ and $\hat{h}$, and mean angle of attack $\bar{\alpha}$ are presented in Tables 3a and 3b, respectively.

Table 2: Initial values of the computations

method	M_c	α_c $[^o]$	α_{0c} $[^o]$
Exp.$_a$	0.768	1.28	1.91
SA$_b$	0.753	-0.08	0.60

$_a$ = without wind tunnel corrections.
$_b$ = with transition.

Table 3a: Flutter result

method	$\bar{\alpha}$ $[^o]$	$\hat{\alpha}$ $[^o]$	$\hat{h}$ $[mm]$
Exp.$_a$	1.28	0.18	0.65
SA$_b$	-0.160	4.09	10.5

Table 3b: Flutter result

method	f $[Hz]$	Φ $[^o]$
Exp.$_a$	32.85	176.7
SA$_b$	33.42	169.8

CONCLUSIONS

Good agreement with the measured time-averaged pressure distribution could be obtained after correcting the free-stream Mach number and the angle of attack for wind-tunnel interference effects. The Baldwin-Barth and the Spalart-Allmaras turbulence models in combination with the Gostelow transition model yielded the best agreement.

Using the Spalart-Allmaras turbulence model, the transonic, two-degree-of-freedom bending/torsion flutter analysis of the NLR 7301 supercritical airfoil section predicted limit-cycle flutter. The phase angle between pitch and plunge and the flutter frequency match the experimental values quite well, but the computed flutter amplitude exceeded the measured amplitude by an order of magnitude. Incorporation of the transition model did not significantly affect this result. This discrepancy between the measured and the computed amplitudes could be due to the following reasons:

a. Omission of unsteady wind-tunnel interference effects.
b. Incorrectly chosen corrected free-stream Mach number.
c. Incorrectly chosen corrected spring-neutral angle of attack.
d. Insufficient resolution of the shock location.
e. Insufficient resolution of transition onset.
f. Insufficient knowledge about transition onset.

These aspects need to be further investigated.

ACKNOWLEDGMENT

The first author gratefully acknowledges the support of the Deutsche Forschungsgemeinschaft (DFG) and the Naval Postgraduate School. Also, the authors are indebted to Dr. A. Knipfer at the DLR Goettingen, Germany. NAVO provided computing time on the DoD High Performance Computing Systems.

REFERENCES

Baldwin, B.S. and Lomax,H., "Thin Layer Approximation and Algebraic Model for Separated Turbulent Flow," AIAA 16th Aerospace Science Meeting, Huntsville, Alabama, 1978

Baldwin, B.S., and Barth, T.J., "A One-Equation Turbulence Transport Model for High Reynolds Number Wall-Bounded Flows," NASA TM 102847, 1990

Cebeci, T., and Bradshaw, P., "Momentum Transfer in Boundary Layers," Hemisphere Publishing Corporation, 1977

Chakravarthy, S.R. and Osher, S., "Numerical Experiments with the Osher Upwind Scheme for the Euler Equations," **AIAA Journal**, Vol. 21, No. 11, 1983, pp. 1241-1248.

Ekaterinaris, J.A., Sorensen, N.N., and Rasmussen, F., " Numerical Investigation of Airfoil Dynamic Stall in Simultaneous Harmonic Oscillatory and Translatory Motion," **ASME Journal of Solar Energy Engineering**, Vol. 120, pp 75-83, 1998

Ekaterinaris, J.A., Platzer, M.F., "Computational Prediction of the Airfoil Dynamic Stall," **Prog. Aerospace Sci.** Vol. 33, pp. 759-846, 1997

Ekaterinaris, J.A., Platzer, M.F., " Numerical Investigation of Stall Flutter," **Journal of Turbomachinery**, Vol. 118, pp 197-203, 1996

Ekaterinaris, J.A., Cricelli, A.S., and Platzer, M.F., " A Zonal Method for Unsteady, Viscous, Compressible Airfoil Flows," **Journal of Fluids and Structures**, Vol. 8, pp. 107-123, 1994

Ekaterinaris, J.A., Menter, F.R., "Computation of Oscillating Airfoil Flows with One- and Two-Equation Turbulence Models," **AIAA Journal**, Vol. 32, No. 12, pp. 2359-2365, 1994

Gostelow, J.P., Melwani, N., and Walker, G.J., "Effects of a Streamwise Pressure Gradient on Turbulent Spot Development," **ASME Journal of Turbomachinery**, Vol. 118, pp.737-747, 1996

Jones, K.D., and Platzer, M.F. "Airfoil Geometry and Flow Compressibility Effects on Wing and Blade Flutter," AIAA 98-0517, Reno, 1998

Knipfer, A., Schewe, G., Wendt, V. "Numerische und experimentelle Untersuchungen an einem schwingenden NLR7301-Profil in transsonischer Stroemung, Teil 1: Flattern und erzwungene Schwingungen," DLR Bericht IB 232-98 J 05, 1998

Osher, S. and Chakravarthy, S.R., "A New Class of High Accuracy TVD Schemes for Hyperbolic Conservation Laws," AIAA Paper 85-0363, 1985.

Rai, M.M. and Chakravarthy, S.R., "An Implicit Form of the Osher Upwind Scheme," **AIAA Journal**, Vol. 24, No. 5, May, 1988, pp. 735-743.

Sanz, W., and Platzer, M.F., "On the Navier-Stokes Calculation of Separation Bubbles With a New Transition Model," **Transaction of the ASME**, Vol. 120, pp 36-42, 1998

Schewe, G., and Deyhle, H., "Experiments on Transonic Flutter of a Two-Dimensional Supercritical Wing with Emphasis on the Non-Linear Effect," Proceedings of the Royal Aeronautical Society Conference on Unsteady Aerodynamics, London, 1996

Spalart, P.R., Allmaras, S.R., "A One-Equation Turbulence Model for Aerodynamic Flows," AIAA Paper 92-0439, 1992

Steger, J. L. and Warming, R. F., "Flux Vector Splitting of the Inviscid Gas Dynamic Equations with Applications to Finite-Difference Methods," **Journal of Computational Physics**, Vol. 40, 1981, pp. 263-293.

Van Dyken, R.D., Ekaterinaris, J.A., Chandrasekhara, M.S., and Platzer, M.F., "Analysis of Compressible Light Stall Flow at Transitional Reynolds Numbers," **AIAA Journal**, Vol. 34, No. 7, pp. 1420-1427, 1996